

# Superfast maximum likelihood reconstruction for quantum tomography

Jiangwei Shang,<sup>1</sup> Zhengyun Zhang,<sup>2,\*</sup> and Hui Khoo Ng<sup>1,3,4</sup>

<sup>1</sup>Centre for Quantum Technologies, National University of Singapore, Singapore 117543, Singapore

<sup>2</sup>BioSyM IRG, Singapore-MIT Alliance for Research and Technology (SMART) Centre, Singapore 138602, Singapore

<sup>3</sup>Yale-NUS College, Singapore 138527, Singapore

<sup>4</sup>MajuLab, CNRS-UNS-NUS-NTU International Joint Research Unit, UMI 3654, Singapore

(Posted on the arXiv on July 3, 2022)

Conventional methods for computing maximum-likelihood estimators (MLE) often converge slowly in practical situations, leading to a search for simplifying methods that rely on additional assumptions for their validity. In this work, we provide a fast and reliable algorithm for maximum likelihood reconstruction that avoids this slow convergence. Our method utilizes an accelerated projected gradient scheme that allows one to accommodate the quantum nature of the problem in a different way than in the standard methods. We demonstrate the power of our approach by comparing its performance with other algorithms for  $n$ -qubit state tomography. In particular, an 8-qubit situation that purportedly took weeks of computation time in 2005 can now be completed in under a minute for a single set of data, with far higher accuracy than previously possible. This refutes the common claim that MLE reconstruction is slow, and reduces the need for alternative methods that often come with difficult-to-verify assumptions. The same algorithm can be applied to general optimization problems over the quantum state space; the philosophy of projected gradients can further be utilized for optimization contexts with general constraints.

*Introduction.*— Efficient and reliable characterization of properties of a quantum system, for example, its state or the process it is undergoing, is needed for the success of any quantum information processing task. Such are the goals of quantum tomography [1], broadly classified into state tomography and process tomography. Process tomography can be recast as state tomography via the well-known Choi-Jamiołkowski isomorphism [2, 3]; we hence restrict our attention to state tomography. Tomography is a two-step process: the first is data gathering via appropriate measurements of the quantum system; the second is the estimation of the state from the gathered data. This second step is the focus of this article.

A popular estimation strategy is that of the maximum-likelihood estimator (MLE) [4] from standard statistics, a matter of convex optimization. Computing the MLE for quantum tomography is, however, not straightforward due to the constraints imposed by quantum mechanics. While general-purpose and easy-to-use convex optimization toolboxes (e.g., CVX [5, 6]) are available for small-sized problems, it is clear that specially adapted MLE algorithms are needed for tackling useful system sizes. Past MLE algorithms [7, 8] incorporate the quantum constraints by going to the *factored space* (see definition later) where the quantum constraints are satisfied by construction via a many-to-one map back to the state space. Gradient methods can then be straightforwardly employed in the now-unconstrained factored space. These algorithms can be slow in practice, with an extreme example [9] of an 8-qubit situation purportedly (see Refs. [10–12]) requiring *weeks* of computation time, to find the MLE, together with bootstrapped error bars (10 MLE reconstruction in all), for the measured

data [13]. This has triggered a search for alternative approaches to MLE reconstruction [10–12, 14], specializing to circumstances in which certain assumptions about the system are applicable, permitting simpler and hence, faster, reconstruction.

Yet, the MLE approach provides a principled estimation strategy, and is still one of the most popular methods for experimenters. The MLE gives a justifiable point estimate for the state [15]. It is the natural starting point for different ways of quantifying the uncertainty in the estimate: One can bootstrap the measured data [16] and quantify the scatter in the MLEs for simulated data; confidence regions can be established starting from the MLE point estimator (this is standard in statistics, but a recent discussion can be found in [17]); credible regions for the actual data are such that the MLE is the unique state contained in every error region [18]. It is thus worthwhile to pursue better methods for finding the MLE.

Here, we present a fast algorithm to accurately compute the MLE from tomographic data. The computation of the MLE for a single set of data for the 8-qubit situation mentioned above now takes less than a minute, and returns a far more accurate answer than previous algorithms in the same amount of time. The speedup and accuracy originate from two features introduced here: (i) the “CG-APG” algorithm that combines an accelerated projected-gradient (APG) approach, which overcomes convergence issues of previous methods, with the existing conjugate-gradient (CG) algorithm; (ii) the use of the product structure (if present) of the tomographic measurements to speed up each iterative step. The CG-APG algorithm gives faster and more accurate reconstruction whether or not the tomographic measurements are of product structure; the product structure, if present, can also be employed to speed up previous MLE algorithms.

\* Corresponding email: zhengyun@smart.mit.edu

*The problem setup.*— In a typical quantum tomography scenario,  $N$  independently and identically prepared copies of the quantum state are measured one-by-one via a set of measurement outcomes  $\{\Pi_k\}_{k=1}^K$ , with  $\Pi_k \geq 0 \forall k$  and  $\sum_{k=1}^K \Pi_k = \mathbf{1}$ .  $\{\Pi_k\}_{k=1}^K$  is formally known as a POM (positive operator-valued measure) or a POM (probability-operator measurement). The measured data  $D$  consist of a sequence of detection events  $\{e_1, e_2, \dots, e_N\}$ , where  $e_\alpha = k$  records the click of the detector for outcome  $\Pi_k$  for the  $\alpha$ th copy measured. The likelihood for data  $D$  given state  $\rho$  is

$$L(D|\rho) = \prod_k p_k^{n_k} = \left\{ \prod_k [\text{tr}(\rho \Pi_k)]^{f_k} \right\}^N, \quad (1)$$

where  $p_k = \text{tr}(\rho \Pi_k)$  is the probability for outcome  $\Pi_k$ ,  $n_k$  is the total number of clicks in detector  $k$ , and  $f_k = n_k/N$  is the relative frequency.

The MLE strategy views the likelihood as a function of  $\rho$  for the obtained  $D$ , and identifies the quantum state  $\rho$  (the statistical operator or density matrix), with  $\rho \geq 0$  and  $\text{tr}(\rho) = 1$ , that maximizes  $L(D|\rho)$  as the best guess—the MLE  $\hat{\rho}_{\text{ML}}$ . This can be phrased as an optimization problem for the normalized negative log-likelihood,  $F(\rho) \equiv -\frac{1}{N} \log L(D|\rho)$ :

$$\underset{\rho \in \mathcal{B}(\mathcal{H})}{\text{minimize}} \quad F(\rho) = -\sum_{k=1}^K f_k \log(\text{tr}(\rho \Pi_k)), \quad (2a)$$

$$\text{subject to} \quad \rho \geq 0 \quad \text{and} \quad \text{tr}(\rho) = 1. \quad (2b)$$

The domain here is the space of bounded operators  $\mathcal{B}(\mathcal{H})$  on the  $d$ -dimensional Hilbert space  $\mathcal{H}$ . We refer to (2b) as the quantum constraints. Any  $\rho \in \mathcal{B}(\mathcal{H})$  satisfying (2b) is a valid state; the convex set of all valid states is the quantum state space.  $F$  is convex, and hence has a unique minimum value, on the quantum state space. Furthermore,  $F(\rho)$  is differentiable (except at isolated points) with gradient  $\nabla F(\rho) = -\sum_{k=1}^K \Pi_k f_k / p_k \equiv -R$ , so that  $\delta F(\rho) \equiv F(\rho + \delta\rho) - F(\rho) = \text{tr}(\delta\rho \nabla F) = -\text{tr}(\delta\rho R)$  for infinitesimal unconstrained  $\delta\rho$ .

*The problem of slow convergence.*— Previous MLE algorithms [7, 8] converge slowly to the MLE because of the “by-construction” incorporation of the quantum constraints (2b): One writes  $\rho = A^\dagger A / \text{tr}(A^\dagger A)$  for  $A \in \mathcal{B}(\mathcal{H})$ , and performs gradient descent in the *factored space* of unconstrained  $A$  operators, for  $\tilde{F}(A) \equiv F(\rho = A^\dagger A / \text{tr}(A^\dagger A))$ . Straightforward algebra yields

$$\delta \tilde{F}(A) = -\text{tr} \left( \delta A \frac{(R-1)A^\dagger}{\text{tr}(A^\dagger A)} + h.c. \right). \quad (3)$$

to linear order in  $\delta A$ .  $\delta \tilde{F}(A)$  is negative—hence walking downhill—for  $\delta A = \epsilon A(R-1)$ , for a suitably chosen small  $\epsilon$ . This choice of  $\delta A$  prescribes a  $\rho$ -update of the form

$$\rho_i \rightarrow \rho_{i+1} = \rho_i + \delta\rho_i, \quad \text{with} \quad \delta\rho_i = \epsilon[(R-1)\rho_i + \rho_i(R-1)] \quad (4)$$

to linear order in  $\epsilon$ .  $\delta\rho_i$  comprises two terms, each with  $\rho_i$  as a factor. When the MLE is close to the boundary of the state space—a typical situation when there are limited data (unavoidable in high dimensions) for nearly pure true states— $\rho_i$  eventually gets close to a rank-deficient state and has at least one small eigenvalue. Yet,  $\rho_i$  has unit trace, so its spectrum must be highly asymmetric.  $\delta\rho_i$  inherits this asymmetry, leading to a locally ill-conditioned problem and slow convergence.

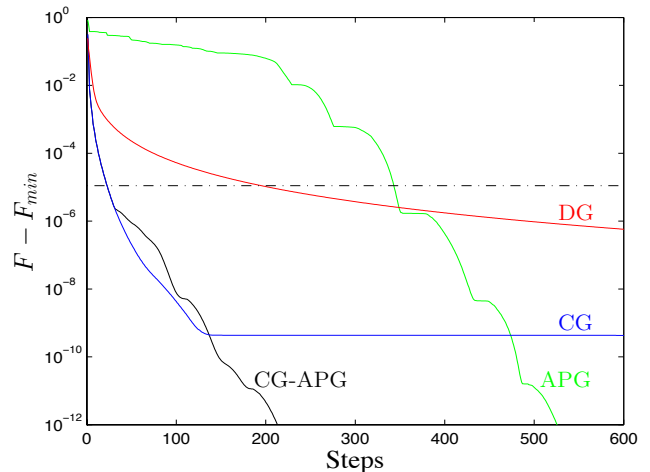


FIG. 1. The deviation  $F - F_{\text{min}} = -\frac{1}{N} \log(L/L_{\text{max}})$  at each step of the iteration for different algorithms, for the experimental data of [9].  $F_{\text{min}}$  is the smallest  $F$  value attained among the algorithms when run till further progress is hindered by machine precision;  $L_{\text{max}}$  is the corresponding likelihood value. Here,  $N = 3^8 \times 100$ , for 100 copies for each of the  $3^8$  settings of the 8-qubit product-Pauli POM. The dash-dotted line indicates the  $F$  value obtained in [9] with the DG algorithm.

To illustrate, consider the situation of [9]: tomography of a (target) 8-qubit  $W$ -state via product-Pauli measurements. Figure 1 shows the trajectories taken by different algorithms from the maximally mixed state to the MLE—the minimum of  $F$ —for the experimental data of [9]. The red and blue lines are for commonly used MLE methods: the diluted direct-gradient (DG) algorithm [7] and the CG algorithm with step-size optimization via line search [8]. Both algorithms walk in the factored space, with DG performing straightforward descent according to Eq. (4), while CG walks along the conjugate-gradient direction. The plot shows the DG and CG iterations initially decreasing  $F$  quickly, but the advances soon stall, with  $F$  stagnating at values significantly larger than attainable by the APG and CG-APG algorithms (explained below). Note that on average the CG-APG and DG algorithms take about the same time per iterative step; see Appendix A for a graph similar to Fig. 1 but plotted against time rather than steps.

*The CG-APG algorithm.*— The slowdown in convergence for DG and CG puts a severe limit on the accuracy of the MLE reconstruction: The analysis of [9]

stopped—after a long wait [13]—at a state with likelihood  $L \simeq 0.1\%L_{\max}$ . That was sufficient for the purpose of [9] to show the establishment of entanglement, but can hardly be considered useful for further MLE analysis. The ill-conditioning in the factored space, which leads to the slowdown in DG and CG, can be avoided by walking in the  $\rho$ -space. There,  $F(\rho)$  has gradient  $R$  which, unlike that of  $\tilde{F}(A)$ , is not proportional to  $\rho$ . Walking in the  $\rho$ -space, however, does not ensure the quantum constraints (2b) are satisfied. The constraints are instead enforced by projecting the unconstrained  $\rho$  operator back into the quantum state space after each gradient step. This is an example of the well-studied and often-used “projected-gradient” methods in numerical optimization [19–21].

In steepest-descent methods, the local condition number of the merit function [ $F(\rho)$  or  $\tilde{F}(A)$  here] affects convergence. Poor conditioning leads to a steepest-descent direction that oscillates back and forth. One smooths out the approach to the minimum by giving each step some “momentum” from the previous step. The CG method implements this for quadratic merit functions; for projected gradients, accelerated gradient schemes [22] are instead the focus. Coupled with adaptive restart [23], the APG method can be thought of as indirectly probing the local condition number by gradually increasing the amount of momentum preserved (controlled by  $\theta$  in the algorithm below), and resetting ( $\theta = 1$ ) whenever the momentum causes the current step to point too far from the steepest-descent direction. The APG algorithm of Refs. [22–24], in  $\rho$ -space, thus proceeds as follows:

---

**Algorithm: APG with adaptive restart**

---

Given  $\rho_0$ ,  $0 < \beta < 1$ , and  $t_1 > 0$ .  
Initialize  $\varrho_0 = \rho_0$ ,  $\theta_0 = 1$ .

**for**  $i = 1, \dots$ , **do**  
  Set  $t_i = t_{i-1}$ ,  $\rho_i = \text{proj}(\varrho_{i-1} - t_i \nabla F(\varrho_{i-1}))$ ,  $\delta_i = \rho_i - \varrho_{i-1}$ .  
  (Choose step size via backtracking)  
  **while**  $F(\rho_i) > F(\varrho_{i-1}) + \langle \nabla F(\varrho_{i-1}), \delta_i \rangle + \frac{1}{2t_i} \|\delta_i\|_F^2$  **do**  
    Set  $t_i = \beta t_i$ .  
    Update  $\rho_i = \text{proj}(\varrho_{i-1} - t_i \nabla F(\varrho_{i-1}))$ ,  $\delta_i = \rho_i - \varrho_{i-1}$ .  
  **end while**  
  Set  $\hat{\delta}_i = \rho_i - \rho_{i-1}$ ; Termination criterion.  
  **if**  $\langle \delta_i, \hat{\delta}_i \rangle < 0$  **then** (Restart)  
     $\rho_i = \rho_{i-1}$ ,  $\varrho_i = \rho_{i-1}$ ,  $\theta_i = 1$ ;  
  **else** (Accelerate)  
    Set  $\theta_i = \frac{1}{2} \left( 1 + \sqrt{1 + 4\theta_{i-1}^2} \right)$ ,  $\varrho_i = \rho_i + \hat{\delta}_i \frac{\theta_{i-1} - 1}{\theta_i}$ .  
  **end if**  
**end for**

---

The operation  $\text{proj}(\cdot)$  above projects the Hermitian argument to the nearest state [satisfying constraints (2b)] as measured by the Euclidean distance [11]. One can also modify the backtracking portion of the algorithm for better performance; see Appendix B for further details.

Applying the APG algorithm to the 8-qubit example above, one indeed finds fast convergence to the MLE (see

Fig. 1) once the walk brings us sufficiently close; no slowdown of convergence as seen in DG and CG is observed. APG with adaptive restart exhibits linear convergence (i.e., the deviation from the optimal value decreases exponentially) in areas of strong convexity [23] sufficiently close to the minimum point.

Far from the minimum, APG can descend slowly, as is clearly visible in Fig. 1. CG descent in the factored space, on the other hand, is rapid in this initial phase. Similar behavior is observed for other states (see a representative example in Appendix C), although the initial slow APG phase is usually markedly shorter than in the  $W$ -state example here. Thus, a practical strategy is to start with CG in the factored space to capitalize on its initial rapid descent, and switch over to APG in the  $\rho$ -space when the fast convergence of APG sets in, *provided* one can determine cheaply when the switch should occur.

Both the APG and CG algorithms use a local quadratic approximation at each step, the accuracy of which relies on the local curvature, measured by the Hessian of the merit function. The advance is quick if the Hessian changes slowly from step to step so that prior-step information provides good guidance for the next step. Empirically, for nearly pure true states, we observe that the Hessian of  $F(\rho)$  changes a lot initially in the APG algorithm but settles down close to the MLE. This is likely a consequence of the fact that the APG trajectory comes very quickly close to the boundary of the state space, so that some  $p_k$  values, which occur in the Hessian of  $F(\rho)$  as  $\sim f_k/p_k^2 \equiv h_k$ , can be very small and unchecked by the  $f_k$  values away from the MLE. On the other hand, the Hessian of  $\tilde{F}(A)$  relevant for the CG algorithm is initially slowly changing, but starts fluctuating closer to the MLE, likely due to the ill-conditioning in the factored-space gradient discussed previously. With this understanding, the proposal is then to start with CG in the factored space, perform a test along the way to detect when the Hessian of  $F(\rho)$  settles down, at which point one switches over to APG in the  $\rho$ -space for rapid convergence to the minimum. The Hessian itself is, however, expensive to compute; one can instead get a good gauge by monitoring the different  $h_k$  values, cheaply computable from the  $p_k$ s already used in the algorithm; see Appendix A. This then is finally our CG-APG algorithm, with a superfast approach to the MLE that outperforms all other algorithms; see Fig. 1.

*Exploiting the product structure.*— Part of the speed in the computation of the MLE in the 8-qubit example above stems from exploiting the product structure of the situation. For the four algorithms compared, the most expensive part of the computation is the evaluation of the probabilities  $\{p_k = \text{tr}(\rho \Pi_k)\}$  needed in  $F$  and  $\nabla F = -R$ , for  $\rho$  at each iterative step. For a  $d$ -dimensional system and  $K$  POM outcomes, the computational cost for obtaining the full set of  $p_k$ s is  $O(Kd^2)$  [there are  $K$  probabilities, each requiring  $O(d^2)$  operations for the trace of a product of two  $d \times d$  matrices]. For the 8-qubit example,  $d = 2^8 = 256$ , and the POM has  $K = 6^8 = 1679616$

outcomes.

The computational cost can be greatly reduced if one has a product structure: The system comprises  $n$  registers, and the POM is a product of individual POMs on each register. For simplicity, we assume the  $n$  registers each have dimension  $d_r$ , and the POM on each register is the same, written as  $\{\pi_k\}_{k=1}^{K_r}$ . The  $n$ -register POM outcome is then  $\Pi_{\vec{k}} = \pi_{k_1} \otimes \pi_{k_2} \otimes \dots \otimes \pi_{k_n}$ , with  $\vec{k} \equiv (k_1, k_2, \dots, k_n)$  and  $k_a = 1, \dots, K_r$ . The generalization to non-identical registers and POMs is obvious. The total dimension is  $d = d_r^n$  and  $K = K_r^n$ . Exploiting this product structure reduces the computational cost of evaluating the probabilities from  $O(K_r^n d_r^{2n})$  to  $O(K_r^{n+1})$  (for  $K_r > d_r^2$ ). For  $n$  qubits with product-Pauli measurements ( $d_r = 2$ ,  $K_r = 6$ ), this is a huge reduction from  $\sim 6^n 4^n$  to  $\sim 6^{n+1}$ .

The computational savings arise because parts of the evaluation of the probabilities can be re-used. Let  $\rho_{n-1}^{(k_n)} \equiv \text{tr}_n(\rho \pi_{k_n})$ , the partial trace on the  $n$ th register, for a given  $k_n$ . This same  $\rho_{n-1}^{(k_n)}$  can be used to evaluate  $\rho_{n-2}^{(k_{n-1}, k_n)} \equiv \text{tr}_{n-1}(\rho_{n-1}^{(k_n)} \pi_{k_{n-1}})$  for any  $k_{n-1}$ . One does this repeatedly, partial-tracing out the last register each time, until one arrives at the probabilities  $p_{\vec{k}} = \rho_0^{(k_1, k_2, \dots, k_n)}$ . At each stage, evaluating  $\rho_{\ell-1}^{(k_\ell, \dots, k_n)}$  from  $\rho_{\ell}^{(k_{\ell+1}, \dots, k_n)}$  involves computing the trace of  $\pi_{k_\ell}$  with submatrices of  $\rho_{\ell}^{(k_{\ell+1}, \dots, k_n)}$ . Specifically,

$$\rho_{\ell}^{(k_{\ell+1}, \dots, k_n)} = \sum_{\vec{i}^{(\ell-1)}, \vec{j}^{(\ell-1)}} |\vec{i}^{(\ell-1)}\rangle \langle \vec{j}^{(\ell-1)}| \otimes \rho_{\vec{i}^{(\ell-1)}, \vec{j}^{(\ell-1)}}, \quad (5)$$

where  $\vec{i}^{(\ell-1)} \equiv (i_1, i_2, \dots, i_{\ell-1})$  with  $i_a = 1, \dots, d_r$  (similarly for  $\vec{j}^{(\ell-1)}$ ),  $\rho_{\vec{i}^{(\ell-1)}, \vec{j}^{(\ell-1)}}$  is a  $d_r \times d_r$  submatrix, and the full  $\rho_{\ell}^{(k_{\ell+1}, \dots, k_n)}$  is a  $(d_r)^{\ell-1} \times (d_r)^{\ell-1}$  array of these submatrices. Getting  $\rho_{\ell-1}^{(k_\ell, \dots, k_n)}$  from  $\rho_{\ell}^{(k_{\ell+1}, \dots, k_n)}$  simply requires replacing each submatrix in  $\rho_{\ell}^{(k_{\ell+1}, \dots, k_n)}$  by the number  $\text{tr}(\rho_{\vec{i}^{(\ell-1)}, \vec{j}^{(\ell-1)}} \pi_{k_\ell})$ , which takes  $O(d_r^2)$  computations. Since each  $\rho_{\ell}^{(k_{\ell+1}, \dots, k_n)}$  need only be computed once for all subsequent  $k_{j \leq \ell}$ , simple counting (see Appendix D) yields a total computational cost of  $O(K_r^{n+1})$  (for  $K_r > d_r^2$ ) to evaluate the full set of probabilities.

Figure 2 shows the performance of the different algorithms for a varying number of qubits with and without exploiting the product structure, for the product-Pauli measurement. A significant speedup is visible when the product structure is incorporated. Similar behavior is observed for the commonly used alternative POM, the product-tetrahedron measurement [25]. For comparison, we also display the runtime for the general-purpose CVX toolbox for convex optimization [5, 6]; the clear disadvantage there is the inability to capitalize on the product structure. Note that CVX does not allow direct specification of a convergence criterion on the  $L$  value as we have done in the other algorithms; the plotted points are instead verified after the fact to have an average  $L$

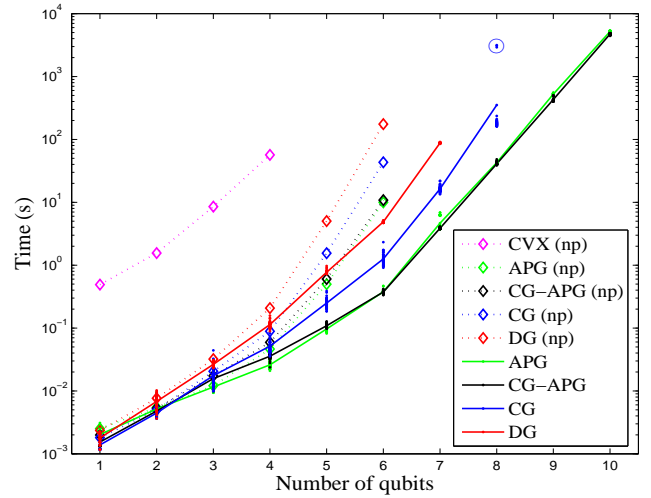


FIG. 2. (Color only.) Time taken, for a convergence criterion of  $L/L_{\max} = 99\%$ , for different algorithms on a varying number of qubits  $n$ . For each  $n$ , 50 states are used, each a Haar-random pure state with 10% added white noise to emulate a noisy preparation. For each state, the different algorithms are run for  $\{f_k = p_k\}$ , where  $\{p_k\}$  are the Born probabilities for the state on the  $n$ -qubit product-Pauli POM. The MLE is hence the actual state. The lines labeled “np” indicate runs *without* using the product structure. These stop at six qubits due to the long time taken. The lines are drawn through the average time taken for each algorithm over the 50 states; the scatter of the timings are shown only for the algorithms using the product structure. For  $n = 8$ , CG did not converge within the maximum allotted time ( $> 20$  times that taken by CG-APG/APG) in 3 out of the 50 states; these points are plotted with that maximum allotted time (circled points), and the average time taken is hence a lower bound on the actual average for CG. CG failed to converge in a reasonable time for all states beyond 8 qubits; DG failed to converge beyond 7 qubits.

value much less than  $99\%L_{\max}$ . All computations are conducted with *MATLAB* on a desktop computer (3 GHz Intel Xeon CPU E5-1660).

It is important to note that incorporating the product structure in the MLE reconstruction is very different from putting in assumptions about the state or the noise: In the former, one knows the structure by design of the tomographic experiment; the latter assumptions require additional checks of compliance, which cannot be guaranteed to be easy or even possible to do. One should also note that tomography experiments with systems larger than a couple of qubits typically employ POMs with a product structure, because of the comparative ease in design and construction, so this product assumption is very often satisfied in practice.

*Conclusion.*— We have demonstrated that, with the right algorithm, MLE reconstruction can be done quickly and reliably, with no latent restriction on the accuracy of the MLE obtained. As the dimension increases, there is no getting around the fact that any tomographic reconstruction will become very expensive, but our algorithm

slows the onset of that point beyond the system size currently accessible in experiments. We note here that our method can be immediately applied to the reconstruction of the MLE for process tomography. Furthermore, it is a general method for optimization in the quantum state space or other types of constraints, and hence can also be used in other such problems.

This work is funded by the Singapore Ministry of Education (partly through the Academic Research Fund Tier 3 MOE2012-T3-1-009) and the National Research Foundation of Singapore. The research is also supported by the National Research Foundation (NRF), Prime Minister's Office, Singapore, under its CREATE programme, Singapore-MIT Alliance for Research and Technology (SMART) BioSystems and Micromechanics (BioSyM) IRG. HKN is partly funded by a Yale-NUS College start-up grant. The authors thank C. Roos and O. Guhne for sharing the experimental data of Ref. [9] and information about the MLE reconstruction used in that work. ZZ thanks Chenglong Bao for his discussions regarding APG and George Barbastathis for general discussions.

J. Shang and Z. Zhang contributed equally to this work.

### Appendix A: Time taken for 8-qubit trajectories

Here we show again the trajectories taken by different algorithms as in Fig. 1 in the main text, but now plotted against time rather than iterative steps.

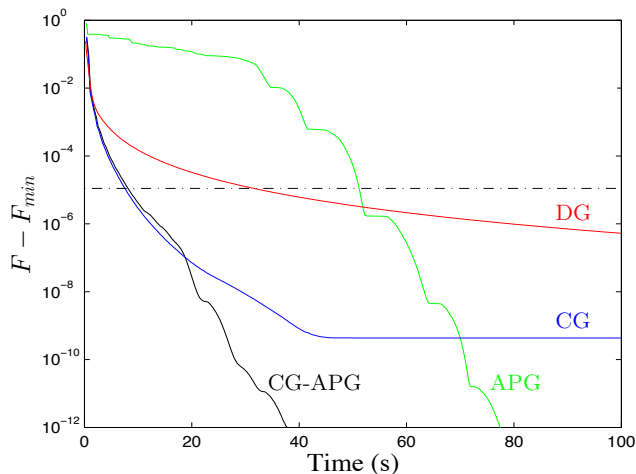


FIG. 3. The deviation  $F - F_{\min} = -\frac{1}{N} \log(L/L_{\max})$  versus time taken for different algorithms, for the experimental data of [9].

### Appendix B: The APG and CG-APG algorithms

We discuss various technical details pertaining to the APG and/or CG-APG algorithms described in the main

text.

#### 1. The projection algorithm used in APG

As explained in the main text, the APG algorithm relies on a projection  $\text{proj}(\cdot)$  to enforce the quantum constraints after each gradient step. The argument of  $\text{proj}(\cdot)$  is a Hermitian operator  $\varrho$  with eigenvalues  $\lambda_i$  (in descending order) and eigenvectors  $|\psi_i\rangle$ . One projects  $\{\lambda_i\}$  onto the probability simplex so that  $\{\lambda_i\} \rightarrow \{\bar{\lambda}_i\}$  with  $\bar{\lambda}_i \geq 0 \forall i$  and  $\sum_i \bar{\lambda}_i = 1$ , and then rebuilds the operator with  $\{\bar{\lambda}_i\}$ , i.e.,  $\text{proj}(\varrho) = \sum_i \bar{\lambda}_i |\psi_i\rangle \langle \psi_i|$ . The projection of  $\lambda_i$  onto the simplex is done as follows [11]: Find  $u = \max \left\{ j : v_j - \frac{1}{j} (\sum_{i=1}^j v_i - 1) > 0 \right\}$ , then define  $w = \frac{1}{u} (\sum_{i=1}^u v_i - 1)$ . Finally we have  $\bar{\lambda}_i = \max\{v_i - w, 0\}$ .

#### 2. Handling negative $p_k$ values

During the gradient step of APG, one can wind up outside the physical state space, i.e.,  $\varrho_i$  at each iterative step need not be a valid state. It can even happen that not all  $p_{k,i} \equiv \text{tr}(\varrho_i \Pi_k)$ s needed in the iterative step are positive, for which  $F(\varrho_i)$  is ill-defined because of the logarithm. We can prevent this by checking whether any  $p_{k,i}$  is negative after  $\varrho_i$  is computed, and set  $\varrho_i = \rho_i$  if this happens to be the case. Empirically, we observe such cases to occur only very rarely.

#### 3. Convergence tweaks for APG

We also incorporated a few small adjustments to APG recommended in Ref. [24], as well as the Barzilai-Borwein method for computing step sizes [26], for better step-size estimation and improved performance in the implementation of the CG-APG algorithm used to produce the figures in the main text. We list those adjustments here.

First, for iterative step  $i > 1$ , rather than fixing the step size as  $t_i = t_{i-1}$ , we set

$$t_i = \frac{\langle \varrho_i - \varrho_{i-1}, \nabla F(\varrho_i) - \nabla F(\varrho_{i-1}) \rangle}{\langle \nabla F(\varrho_i) - \nabla F(\varrho_{i-1}), \nabla F(\varrho_i) - \nabla F(\varrho_{i-1}) \rangle} \quad (\text{B1})$$

if there was no restart in the previous iteration and the denominator is nonzero; otherwise we set  $t_i = \alpha t_{i-1}$ , for some pre-chosen constant  $\alpha$ . We used  $\alpha = 1.1$  and  $\beta = 0.5$  (see main text) as recommended in [24].

We also use the following update on  $\theta_i$  and  $\varrho_i$  for  $i > 1$  to prevent changes in  $t_i$  from affecting convergence:

$$\hat{\theta}_{i-1} = \theta_{i-1} \sqrt{t_{i-1}/t_i} \quad (\text{B2a})$$

$$\theta_i = \frac{1}{2} \left( 1 + \sqrt{1 + 4\hat{\theta}_{i-1}^2} \right) \quad (\text{B2b})$$

$$\varrho_i = \rho_i + \hat{\delta}_i (\hat{\theta}_{i-1} - 1) / \theta_i \quad (\text{B2c})$$

The rules Eqs. (B2b) and (B2c) are exactly those stated in the APG algorithm in the main text, but with  $\theta_{i-1}$  replaced by  $\hat{\theta}_{i-1}$  for the step-size adjustment.

Sometimes we observe that standard APG as prescribed by [23] fails to restart early enough for good performance. We hence use a stricter restart criterion: Restart when

$$\frac{\text{tr}(\delta_i \hat{\delta}_i)}{\sqrt{\text{tr}(\delta_i^2) \text{tr}(\hat{\delta}_i^2)}} < \gamma, \quad (\text{B3})$$

with  $\gamma$  set to a small positive value (0.01 for the graphs in the main text).

#### 4. Switchover criterion for CG-APG

For the CG-APG algorithm, as explained in the main text, one would like to start with CG iterations and switch to APG when the Hessian stabilizes, i.e., it changes only by a little with further APG steps. This happens when the trajectory is sufficiently close to the MLE. Here, we explain the technical details of this switchover.

The Hessian of  $F(\rho)$ —its curvature—characterizes its local quadratic structure. It is the “second derivative” of  $F(\rho)$ , and comes from considering the second-order variation of  $F$ :  $\delta^2 F(\rho) \equiv \delta F(\rho + \tilde{\delta}\rho) - \delta F(\rho)$ , where  $\delta F(\rho) \equiv -\text{tr}(\delta\rho R(\rho))$ , the first-order variation of  $F$ , with  $R(\rho) = \sum_k \Pi_k f_k / p_k$  and  $p_k \equiv \text{tr}(\rho \Pi_k)$  as in the main text. Here,  $\delta\rho$  and  $\tilde{\delta}\rho$  are independent infinitesimal variations of  $\rho$ . A little algebra gives

$$\delta^2 F(\rho) = \text{tr} \left( \delta\rho \sum_k \Pi_k \text{tr} \left( \tilde{\delta}\rho \Pi_k \right) \frac{f_k}{p_k^2} \right), \quad (\text{B4})$$

and we identify the linear operator [on  $\mathcal{B}(\mathcal{H})$ ]

$$H(\rho; \cdot) = \sum_k \Pi_k \text{tr}(\cdot \Pi_k) \frac{f_k}{p_k^2} \quad (\text{B5})$$

as the Hessian of  $F$  at  $\rho$ .

The eigenvalues of  $H$  give the local quadratic structure of  $F(\rho)$ . Ideally, determining the right time during CG to switch to APG requires computing how much  $H$  changes across successive APG steps from the current value of  $\rho$ . However, this would be very costly: It is as if one is running APG alongside CG, and the Hessian is a large matrix ( $d^2 \times d^2$  in size) and hence expensive to compute.

Instead, we adopt a compromise that works well in practice: (1) we treat the  $\Pi_k$ s as if they were all mutually orthogonal so that the eigenvalues of  $H$  would be equal to  $\{f_k/p_k^2\}$ , and (2) we look at the change in  $H$  between iterations of CG instead of between iterations of APG. The  $\Pi_k$ s are never exactly mutually orthogonal for informationally complete measurements, but a good

tomographic design would seek to spread out the  $\Pi_k$  directions, and for large dimensional situations, their mutual overlaps will be small and  $\{f_k/p_k^2\}$  is a good enough proxy for the eigenvalues of the Hessian. While looking at the change in  $H$  across iterations of CG would not always guarantee a similar change for APG, a small change with CG iterations signals closeness to the MLE, or that CG has stagnated. In either case, one should switch to APG.

Thus, in our implementation of CG-APG, we first initialize CG with the maximally mixed state, and switch to APG at the first iteration when the overlap,

$$\frac{\vec{q}_i \cdot \vec{q}_{i-1}}{\sqrt{|\vec{q}_i|^2 |\vec{q}_{i-1}|^2}}, \quad (\text{B6})$$

exceeds  $\cos \phi$  for some chosen small  $\phi$  value. Here,  $\vec{q}_i \equiv (f_1/p_{1,i}^2, f_2/p_{2,i}^2, \dots, f_K/p_{K,i}^2)$ , where  $p_{k,i} = \text{tr}(\rho_i \Pi_k)$  for state  $\rho_i$  of the  $i$ th CG iteration. The switchover thus occurs when the angle between the  $\vec{q}$ s for subsequent iterations is small enough. We find that  $\phi = 0.01$  radians works well in practice.

#### Appendix C: Trajectories for generic states

Figure 1 in the main text shows the trajectories taken by different algorithms for the experimental data of Ref. [9] for a noisy  $W$ -state. There, we saw a long initial slow phase of APG, which is in fact atypical of the behavior seen for generic states. Figure 4 shows the more representative behavior for a random 8-qubit pure state with 10% added white noise. As in Fig. 1,  $N = 3^8 \times 100$ , with 100 copies for each of the  $3^8$  settings of the 8-qubit product-Pauli POM. Observe the significantly shorter length of the initial slow phase of APG than for the noisy  $W$ -state in Fig. 1.

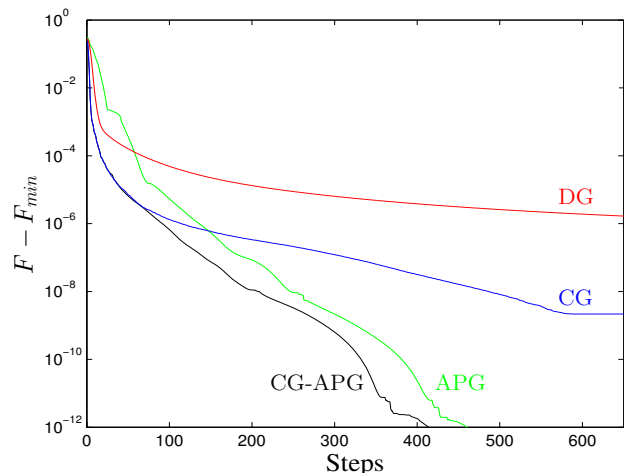


FIG. 4. The plot shows the trajectories taken by different algorithms as in Fig. 1 in the main text, but for simulated data generated from a random 8-qubit pure state with 10% added white noise.

### Appendix D: Exploiting the product structure: Computational savings

Here, we present the counting argument that gives  $O(K_r^{n+1})$  as the computational cost of evaluating a full set of Born probabilities after making use of the product structure of the POM. To remind the reader of the notation: The system comprises  $n$  registers each of dimension  $d_r$ ; the POM on each register is  $\{\pi_k\}_{k=1}^{K_r}$ ; the  $n$ -register POM outcome is  $\vec{\Pi}_{\vec{k}} = \pi_{k_1} \otimes \pi_{k_2} \otimes \dots \otimes \pi_{k_n}$ , with  $\vec{k} \equiv (k_1, k_2, \dots, k_n)$  and  $k_a = 1, \dots, K_r$ ; and  $\rho_{\ell}^{(k_{\ell+1}, \dots, k_n)} \equiv \text{tr}_{\ell+1} \{ \dots \text{tr}_{n-1} \{ \text{tr}_n \{ \rho \pi_{k_n} \} \pi_{k_{n-1}} \} \dots \pi_{k_{\ell+1}} \}$ . We also need the following basic fact: Evaluating  $\text{tr}\{AB\}$  for  $A$  an  $n \times m$  matrix and  $B$  an  $m \times n$  matrix requires  $2mn$  operations (elementary addition/multiplication).

In each step of the procedure described in the main text, one needs to evaluate  $\rho_{\ell-1}^{(k_{\ell}, \dots, k_n)} = \text{tr}_{\ell} \{ \rho_{\ell}^{(k_{\ell+1}, \dots, k_n)} \pi_{k_{\ell}} \}$  for given  $k_{\ell}, \dots, k_n$ . One such eval-

uation requires the computation of the trace of  $\pi_{k_{\ell}}$  with each of the  $(d_r)^{\ell-1} \times (d_r)^{\ell-1}$  submatrices of  $\rho_{\ell-1}^{(k_{\ell+1}, \dots, k_n)}$ .  $\pi_{k_{\ell}}$  and each submatrix are  $d_r \times d_r$  in size, so the computational cost of evaluating  $\rho_{\ell-1}^{(k_{\ell}, \dots, k_n)}$  is  $2d_r^2 \times d_r^{2(\ell-1)} = 2d_r^{2\ell}$  operations. One incurs this cost for every choice of  $k_{\ell}, \dots, k_n$ , so the total cost of evaluating  $\rho_{\ell-1}^{(k_{\ell}, \dots, k_n)}$  for all  $k_{\ell}, \dots, k_n$ , for given  $\ell$ , is  $2K_r^{n-\ell+1} d_r^{2\ell}$ . Adding up this cost over all values of  $\ell = 1, 2, \dots, n$  gives the total cost for evaluating a full set of Born probabilities as

$$\begin{aligned} 2 \sum_{\ell=1}^n K_r^{n-\ell+1} d_r^{2\ell} &= 2K_r^n d_r^2 \sum_{\ell=0}^{n-1} \left( \frac{d_r^2}{K_r} \right)^{\ell} \\ &= 2K_r^n d_r^2 \left[ \frac{1 - (d_r^2/K_r)^n}{1 - (d_r^2/K_r)} \right]. \end{aligned} \quad (\text{D1})$$

For  $K_r > d_r^2$ , as is usually the case, this gives the dominant computational cost of  $O(K_r^{n+1})$ ; for  $K_r = d_r^2$ , one has instead the cost of  $O(nK_r^{n+1})$ .

- 
- [1] M. Paris and J. Řeháček, eds., *Quantum State Estimation*, Lecture Notes in Physics, vol. 649 (Springer-Verlag, Heidelberg, 2004).
- [2] I. L. Chuang and M. A. Nielsen, *J. Mod. Opt.* **44**, 2455 (1997).
- [3] J. F. Poyatos, J. I. Cirac, and P. Zoller, *Phys. Rev. Lett.* **78**, 390 (1997).
- [4] Z. Hradil, J. Řeháček, J. Fiurášek, and M. Ježek, *Maximum-Likelihood Methods in Quantum Mechanics*, Chapter 3 in [1].
- [5] M. Grant and S. Boyd, CVX: Matlab software for disciplined convex programming, version 2.1 (2015).
- [6] M. Grant and S. Boyd, *Graph implementations for non-smooth convex programs*, in V. Blondel, S. Boyd, and H. Kimura, eds., *Recent Advances in Learning and Control*, Lecture Notes in Control and Information Sciences, (Springer, 2008).
- [7] J. Řeháček, Z. Hradil, E. Knill, and A. I. Lvovsky, *Phys. Rev. A* **75**, 042108 (2007).
- [8] Y. S. Teo, *Numerical Estimation Schemes for Quantum Tomography*, Ph.D. thesis (Singapore, 2012); available as eprint arXiv:1302.3399 [quant-ph] (2013).
- [9] H. Häffner, W. Hänsel, C. F. Roos, J. Benhelm, D. Chek-al-kar, M. Chwalla, T. Körber, U. D. Rapol, M. Riebe, P. O. Schmidt, C. Becher, O. Gühne, W. Dür, and R. Blatt, *Nature* (London) **438**, 643 (2005).
- [10] D. Gross, Y.-K. Liu, S. T. Flammia, S. Becker, and J. Eisert, *Phys. Rev. Lett.* **105**, 150401 (2010).
- [11] J. A. Smolin, J. M. Gambetta, and G. Smith, *Phys. Rev. Lett.* **108**, 070502 (2012).
- [12] Z. Hou, H.-S. Zhong, Y. Tian, D. Tong, B. Qi, L. Li, Y. Wang, F. Nori, G.-Y. Xiang, C.-F. Li, and G.-C. Guo, *New J. Phys.* **18**, 083036 (2016).
- [13] C. Roos and O. Gühne, private communication.
- [14] T. Baumgratz, D. Gross, M. Gramer, and M. B. Plenio, *Phys. Rev. Lett.* **111**, 020401 (2013).
- [15] Z. Hradil, *Phys. Rev. A* **55**, R1561 (1997).
- [16] B. Efron and R. J. Tibshirani, *An Introduction to the Bootstrap*, Chapman & Hall, London (1994).
- [17] J. VanderPlas, Proc. of the 13th Python in Science Conf., eds. S. van der Walt and J. Bergstra, pp. 90 (2014) (arXiv:1411.5018 [astro-ph.IM]).
- [18] J. Shang, H. K. Ng, A. Sehwat, X. Li, and B.-G. Englert, *New J. Phys.* **15**, 123026 (2013).
- [19] R. J. Bruck, *J. Math. Anal. Appl.* **61**, 159 (1977).
- [20] G. B. Passty, *J. Math. Anal. Appl.* **72**, 383 (1979).
- [21] Y. Nesterov, *Introductory Lectures on Convex Optimization: A Basic Course*, Kluwer Academic, Dordrecht (2004).
- [22] A. Beck and M. Teboulle, *SIAM J. Imaging Sci.* **2**, 183 (2009).
- [23] B. O'Donoghue and E. Candès, *Found. Comput. Math.* **15**, 715 (2015).
- [24] S. R. Becker, E. Candès, and M. C. Grant, *Math. Prog. Comp.* **3**, 165 (2011).
- [25] J. Řeháček, B.-G. Englert, and D. Kaszlikowski, *Phys. Rev. A* **70**, 052321 (2004).
- [26] J. Barzilai and J. M. Borwein, *IMA J. Numer. Anal.* **8**, 141 (1988).